Cellular polarity asymmetrically functionalizes pathogen recognition receptor-mediated intrinsic immune response in human intestinal epithelium cells

Megan L. Stanifer[1#], Stephanie Muenchau[1], Markus Mukenhirn[1], Kalliopi Pervolaraki[1], Takashi Kanaya[3], Dorothee Albrecht[1], Charlotte Odendall[4], Thomas Hielscher[5], Volker Haucke[6], Jonathan Kagan[7], Sina Bartfeld[8], Hiroshi Ohno[3], Steeve Boulant[1,2#]

[1]Schaller research group at CellNetworks, Department of Infectious Diseases, Virology, Heidelberg University Hospital, Germany;

[2] Research Group "Cellular polarity and viral infection", German Cancer Research Center (DKFZ), Heidelberg, Germany;

[3] Laboratory for Intestinal Ecosystem, RIKEN Center for Integrative Medical Sciences, Yokohama, Kanagawa 230-0045, Japan

[4] Department of Infectious Diseases, King's College London, Guy's Hospital, London SE1 9RT, United Kingdom;

[5] Division of Biostatistics, German Cancer Research Center (DKFZ), Heidelberg, Germany

[6] Department of Molecular Pharmacology & Cell Biology, Leibniz-Forschungsinstitut für Molekulare Pharmakologie (FMP); Freie Universität Berlin, Faculty of Biology, Chemistry and Pharmacy, 14195 Berlin, Germany.

[7] Harvard Medical School and Division of Gastroenterology, Boston Children's Hospital, Boston, MA 02115, USA;

[8] Research Centre for Infectious Diseases, Institute for Molecular Infection

26 Biology, Julius Maximilian University of Wuerzburg, Wuerzburg, Germany

27

28 Running Title: Polarized immune response in human intestinal epithelium cells

29

30

31 #Corresponding authors
32 Steeve Boulant, Ph.D.
33 Department of Infectious Disease, Virology
34 Schaller research group at CellNetworks and DKFZ
35 Heidelberg Hospital University
36 Im Neuenheimer Feld 344
37 69120 Heidelberg, Germany
38 Phone: +49 (0) 6221 56 7865
39 Email: s.boulant@dkfz.de

40

41 Megan L. Stanifer, Ph.D.
42 Department of Infectious Disease, Virology
43 Heidelberg Hospital University
44 Im Neuenheimer Feld 344
45 69120 Heidelberg, Germany
46 Phone: +49 (0) 6221 56 7858
47 Email: m.stanifer@dkfz.de

48

49

Summary

Intestinal epithelial cells (IECs) act as a physical barrier separating the commensal-containing intestinal tract from the sterile interior. These cells have found a complex balance allowing them to be prepared for pathogen attacks while still tolerating the presence of bacteria/viral stimuli present in the lumen of the gut. Using primary human IECs, we probed the mechanisms, which allow for such a tolerance. We discovered that viral infection emanating from the basolateral side of IECs elicited a stronger intrinsic immune response as compared to lumenal apical infection. We determined that this asymmetric immune response was driven by the clathrin-sorting adapter AP-1B which mediates the polarized sorting of Toll-like receptor 3 (TLR3) toward the basolateral side of IECs. Mice and human IECs lacking AP-1B showed an exacerbated immune response following apical stimulation. Together these results suggest a model where the cellular polarity program plays an integral role in the ability of IECs to partially tolerate apical commensals while remaining fully responsive against invasive basolateral pathogens.

Keywords: Intrinsic innate immunity, type III interferon, TLR3, cellular polarity, clathrin, AP-1B, lambda interferon, enteric viruses, organoids, intestinal epithelial cells

72 **Introduction**

73 Intestinal epithelial cells (IECs) lining the gastrointestinal tract constitute the
74 primary barrier separating us from the outside environment. These cells protect
75 the human body from enteric bacterial and viral pathogens (Peterson and Artis,
76 2014). They sense and combat these pathogens using Pathogen Recognition
77 Receptors (PRRs) (e.g. the Toll-like receptors (TLRs)) to trigger an intrinsic
78 innate immune response (Pott and Hornef, 2012, Fukata and Arditi, 2013, Arpaia
79 and Barton, 2011, Barton and Medzhitov, 2003). Importantly, IECs are in
80 constant contact with the ever-present microbiota and therefore have developed
81 mechanisms to tolerate the presence of the commensals while maintaining
82 responsiveness against pathogen (Fukata and Arditi, 2013). The intrinsic innate
83 immune response is regulated not only by complex signal transduction pathways
84 downstream of PRRs but also by compartmentalization of these receptors
85 (Odendall and Kagan, 2017, Chow et al., 2015). This compartmentalization is
86 described to be an important mechanism by which cells avoid self-recognition
87 (Yu and Gao, 2015, Kagan and Barton, 2014). In IECs, this compartmentalization
88 of innate immune functions is believed to be even more critical to maintain gut
89 homeostasis (Yu and Gao, 2015). IECs are polarized, they display a unique apical
90 membrane facing the lumen of the gut and a basolateral membrane facing the
91 lamina propria (Yu and Gao, 2015, Rodriguez-Boulan and Macara, 2014). Enteric
92 pathogens and commensals are normally located in the lumen of the gut thereby
93 generally challenging hIECs through their apical membrane. However, when the
94 barrier function is lost, in the presence of invasive pathogens, or during
95 spreading of infection, pathogens and commensals can gain access the
96 basolateral side of hIECs. The concept that PRRs can induce a different signaling

97 depending on whether the pathogen challenges emanate from the apical or
98 basolateral side of hIECs have been pioneered by studying TLR9 and TLR5
99 (Gewirtz et al., 2001, Lee et al., 2006). The mechanisms leading to this polarized
100 immune response have been described to be mediated by a different signal
101 transduction pathway between apical or basolateral stimulation for TLR9 (Lee et
102 al., 2006) and due to the asymmetric distribution of the PRRs in hIECs for TLR5
103 (Gewirtz et al., 2001). The precise intracellular localization of TLRs and, most
104 importantly, which ones are actually expressed in IECs has been a matter of
105 debate (Price et al., 2018). Additionally, how viruses are detected and combatted
106 in human IECs has been largely understudied. It remains unknown whether virus
107 specific PRRs (i.e. TLR3) can be asymmetrically distributed thereby providing
108 IECs the capacity to distinguish between viral infection emanating from the
109 apical or their basolateral side and as a consequence mount a different immune
110 response.

111 In our study, we determined that IECs respond to viral infection in a side
112 specific manner. We could directly correlate this polarized immune response to
113 the asymmetric distribution of TLR3 towards the basolateral side of IECs. We
114 identify the clathrin sorting adaptor protein AP-1 as the key machinery to sort
115 TLR3 to the basolateral side of IECs. Our results suggest a mechanism used by
116 IECs to generate a moderate immune response against stimuli emanating from
117 the physiological lumenal side while remaining fully responsive against invasive
118 pathogens or in conditions of barrier integrity loss where stimuli can access the
119 normally sterile basolateral side.

120

121 **Results**

122 To address the extent by which TLRs act in a polarized manner in intestinal
123 epithelial cells, the model human IEC line T84 cells were polarized on transwells
124 (Madara et al., 1987). Cellular polarization was controlled through
125 immunostaining of the tight junction belt (data not shown and (Stanifer et al.,
126 2016)). The integrity of the epithelial barrier, a pre-requisite for side specific
127 stimulation, was validated by monitoring the Trans-Epithelium Electrical
128 Resistance (TEER) (Sup. Figure 1A) and by controlling the capacity of the hIEC
129 monolayer to block dextran diffusion in a transwell diffusion assay (Sup. Figure
130 1B). These polarized hIECs were used to evaluate the relative expression of each
131 TLR by q-RT-PCR. Results showed that TLR2, 3, 4 and 5 were the most expressed
132 in hIECs (Figure 1A). Following side-specific stimulations by TLR agonists
133 (Figure 1B), the specific response of hIECs was evaluated by monitoring the
134 transcription upregulation of both IL-6 and type III interferon (IFNλ2/3).
135 Stimulation with TLR7, 8 and 9 agonists did not induce an immune response in
136 hIECs which was consistent with their low expression levels (Figure 1A-D).
137 However, these agonists were fully potent in inducing IL-6 production in pBMCs
138 (Sup. Figure 2A). Importantly, while treatments of the cells with TLR2, 3, 4 and 5
139 agonists resulted in the production of IL-6 (and IL-8, data not shown) and
140 IFNλ, basolateral stimulation of the cells by TLR3 agonist induced a significantly
141 higher production of IFNλ compared to apical stimulation (Figure 1C-D). This
142 stronger induction of interferon upon basolateral stimulation with the TLR3
143 agonist was true at any time post-treatment (Figure 1E). This TLR3-specific
144 polarized immune response was not the result of a more efficient update of the

145 agonist from the basolateral side of the cells as quantification revealed that the
146 kinetics of fluorescently labeled TLR3 agonist uptake was identical between the
147 apical and basolateral side of hIECs (Sup. Figure 2B). Together, these results
148 suggest that hIECs can distinguish between apical and basolateral stimulation of
149 TLR3 and adapt their response in a side specific manner.

150

151 **Basolateral viral infection of hIECs induces a stronger immune response**
152 **compared to apical infection.** To control that the polarized TLR3 immune
153 response was not agonist specific we infected hIECs with mammalian reovirus
154 which is actively sensed by TLR3 during infection (Stanifer et al., 2016).
155 Polarized hIECs grown on transwells were infected in a polarized manner
156 (Figure 2A) and virus replication and cellular immune response was followed
157 overtime as function of infection side (apical vs. basolateral). Results showed
158 that the onset of viral replication was identical between apical and basolateral
159 infection. No significant differences between apical and basolateral infection
160 could be detected in the efficacy of virus uptake (Sup. Figure 3A), in the number
161 of cells infected during the primary round of infection (Figure 2B-C), and in viral
162 replication as measured by viral genome load and production of the viral non-
163 structural protein μNS overtime (Sup. Figure 3B-C). However, at late time points
164 and during multiple rounds of infection, apical infection resulted in a higher level
165 of replication and production of progeny viruses (Figure 2D-E and Sup. Figure
166 3C-E). Interestingly, the lower production of *de novo* viruses following
167 basolateral infection correlated with a stronger intrinsic innate immune
168 response at both the RNA and protein level (Figure 2F-H). A similar stronger

169 immune response following basolateral infection was also observed when using
170 a different hIEC cell line (SKCO15) (Le Bivic et al., 1989) (Sup. Figure 4).
171 Additionally, as observed using the TLR3 agonist poly I:C (Figure 1E), basolateral
172 viral infection of hIECs resulted in a higher production of interferon at all times
173 post-infection at both the RNA and protein levels (Sup. Figure 5).

174 This higher production of interferon following basolateral stimulation and
175 infection could be due to an increased RNA stability or sustained transcription.
176 To address this possibility, cells were treated with actinomycin to inhibit new
177 RNA synthesis (Sup. Figure 6A). The half-life of both apical and basolateral
178 IFNλ2/3 transcripts were found to be similar, however basolateral infection lead
179 to a slightly lower half-life of IFNβ1 transcripts compared to apical infection
180 (Sup. Figure 6B-C). These finding argue that the stronger immune response
181 generated upon basolateral challenges is not the result of differences in the
182 stability of the IFN transcripts. To gain a global understanding of the extent by
183 which apical and basolateral infection/stimulation leads to a different immune
184 response hIECs were infected in side specific manner and their transcriptional
185 profiles was analyzed by microarray. Results show that infection from both sides
186 leads to an increase in immune response related genes however, basolateral
187 infection resulted in a greater number of upregulated genes as well as a higher
188 induction of the genes also upregulated upon apical infection (Sup. Figure 7). In
189 addition, KEGG analysis shows that the upregulated genes are predominantly
190 associated with immune response pathways and interferon-mediated responses.
191 (Sup. Figure 7C).

192 All together these data show that hIECs can react in a side specific manner to

193 TLR3 agonist and viral infection. Basolateral infection/stimulation induces a
194 stronger interferon-mediated immune response compared to the same stimuli
195 coming from their apical side.

196 **Primary intestinal cells respond in a side specific manner to TLR3 stimuli.**
197 To validate our findings in human primary cells we exploited human mini-gut
198 organoids. To perform a side specific stimulation/infection, organoids were
199 grown and differentiated on transwells (Figure 3A). Cell differentiation and the
200 integrity of the barrier function was controlled by immunostaining and TEER
201 measurements (Figure 3B and data not shown). Primary hIECs were infected
202 from either their apical or basolateral side. Although infectivity was not side
203 dependent, basolateral infection lead to a stronger production of interferon
204 (Figure 3C-E). Similar findings were observed when performing side specific
205 infection of 3D organoids. Using microinjection, MRV was introduced within the
206 lumen of the organoids to allow for apical infection or juxtaposed at the organoid
207 periphery to promote basolateral infection (Sup Figure 8A). Following validation
208 that our apical and basolateral microinjection approaches led to equivalent
209 infection of the human mini-gut organoids (Sup Figure 8B-C), we confirmed that
210 basolateral infection lead to a stronger production of interferon compared to
211 apical infection (Sup Figure 8D). To investigate whether this polarized immune
212 response also applies to other TLRs, we performed a side specific stimulation
213 with TLR agonist of primary human organoids on transwells. As observed in our
214 T84 cell line, primary hIECs mostly express TLR2, 3, 4 and 5 (Sup. Figure 8E)
215 which was consistent with previous work using murine IECs (Price et al., 2018).
216 Importantly, although these cells responded to the respective agonists (Figure

217 3F-G), they only show a polarized interferon induction upon TLR3 stimulation
218 (Figure 3G). Altogether, our results demonstrate that hIECs respond in an
219 asymmetric manner to TLR3 stimulation.

220 **The clathrin sorting adapter AP-1B mediates the basolateral localization of**
221 **TLR3 in hIECs.** To address whether the polarized response to
222 infection/stimulation was due to a polarized distribution of the pathogen
223 recognition receptor, we performed immunostaining of TLR3 in hIECs. Human
224 organoids were seeded as a 2D monolayer as described above (Figure 3A), and
225 results show that TLR3 was restricted to the basolateral membrane of hIECs
226 (Figure 4A). Similar results were obtained with both T84 cells grown as
227 spheroids and primary hIECs grown as 3D organoids (Figure 4B-C).
228 Quantification revealed that TLR3 was exclusively localized to the basolateral
229 membrane in human organoids and was mostly localized to the basolateral
230 membrane in T84 cells (Figure 4D).

231 The clathrin sorting adapter AP-1 is well known for sorting proteins to the
232 basolateral membrane of polarized cells ((Folsch, 2015). AP-1 comes in two
233 forms; the ubiquitously expressed AP-1A and the epithelial specific AP-1B. To
234 investigate if AP-1B was responsible for both the polarized distribution of TLR3
235 and the polarized immune response, we used shRNA to knock-down AP-1B in
236 our T84 cell line model (Sup. Figure 9A). Immunostaining of TLR3 revealed that
237 upon AP-1B down regulation, TLR3 was re-localized from the basolateral
238 membrane to the apical side of hIECs (Figure 5A-C). Quantification revealed that
239 most of the AP-1B knock-down spheroids display TLR3 at their apical side
240 (Figure 5D). After controlling the barrier function and integrity of AP-1B knock-

241 down hIECs (Sup. Figure 9B-D), WT and AP-1B knock-down cells were infected
242 in a side specific manner with reovirus. As observed before, basolateral infection
243 of WT hIECs resulted in a stronger production of interferon compared to apical
244 infection. Interestingly, knock-down of AP-1B resulted in an inversion of this
245 polarized response leading to a stronger production of interferon upon apical
246 challenges both at the transcript (Figure 6A) and protein level (Sup. Figure 9E).
247 This stronger interferon production upon apical infection of AP-1B knock-down
248 cells fully correlates with the observation that TLR3 is re-localized to the apical
249 side of hIECs (Figure 5A-D). To control that AP-1B knock-down did not impact
250 global TLR mediated signaling, WT and AP-1B knock-down cells were treated
251 with TLR agonists in a side specific manner. No significant differences were
252 observed for TLR2, 4, 5, 7/8-, and 9-mediated signaling upon AP-1B knock-down
253 (Sup. Figure 10). Importantly, similar to viral infection, an inversion of polarized
254 immune response in AP-1B knock-down cells was observed leading to a higher
255 induction of interferon upon apical treatment of the cells with the TLR3 agonist
256 (Figure 6B and Sup. Figure 10B). To validate that the observed increased
257 immune response in AP-1B knock-down cells upon apical challenges was directly
258 mediated by TLR3, we used a pharmacological inhibitor approach. As TLR3
259 requires TRIF as adapter protein to mediate downstream signaling (Yamamoto
260 et al., 2003), we used a TRIF specific inhibitor. Results confirm that the observed
261 immune response generated by hIECs upon viral infection is largely due to TLR3
262 (Sup. Figure 11A). Importantly, inhibition of TLR3-mediated signaling in AP-1B
263 knock-down cells resulted in a strong reduction of immune response upon apical
264 infection (Sup. Figure 11B). These results strongly suggest that the observed
265 inversion of polarized immune response in AP-1B knock-down is directly

266 associated with the re-localization of TLR3 to the apical side of hIECs. All
267 together these data support a model where the clathrin sorting adapter AP-1
268 mediates the polarized sorting of TLR3 in hEICs rendering them more
269 responsive to pathogen challenges emanating from their basolateral side.

270

271 **IECs derived from AP-1B knock-out mice show a reversion of their**
272 **polarized immune response.** To confirm that AP-1B was contributing to the
273 observed polarized immune response we evaluated mice, which express an
274 inducible intestinal specific knock-out of AP-1B (villin-CreER Ap1m2$^{flox/flox}$,
275 (Takahashi et al., 2011)) (Figure 6C). Intestinal organoids were generated from
276 these mice and exploited for apical and basolateral infection as side specific
277 infection is not possible *in vivo*. While apical infection can be mimicked through
278 gavaging of virus, basolateral infection cannot be controlled as intraperitoneal
279 infection will also deliver virus to the surrounding immune cells and stroma cells
280 thereby resulting in an immune response generated not only by IECs but also by
281 other cell types. Organoids generated from villin-CreER Ap1m2$^{flox/flox}$ were
282 treated with or without tamoxifen and the loss of AP-1B was controlled by qPCR
283 (Figure 6C-D) (see method). AP-1B$^{+/+}$ and AP-1B$^{-/-}$ organoids were seeded onto
284 transwells and infected apically or basolaterally with reovirus. The innate
285 immune induction was controlled by q-RT-PCR and confirmed that similar to our
286 T84 cell model and to our human organoids, murine organoids also show a
287 polarized immune response where a basolateral infection leads to a stronger
288 production of IFN compared to an apical one at both the RNA and protein level
289 (Figure 6E-F). Importantly, in AP-1B knock-out murine organoids, an inversion

290 of polarized immune response was observed where apical infection lead to a
291 higher production of interferon compared to basolateral infection (Figure 6E-F).
292 Similar findings were observed when using a TLR3 agonist to induce an immune
293 response in murine organoids further confirming the role of AP-1B in TLR3-
294 mediated polarized interferon induction (Figure 6G-H).

295

296 **Discussion**

297 In this study we unraveled that the extent of the immune response which
298 is generated downstream TLR3 depends on the side (apical vs. basolateral) of
299 infection/stimulation. Precisely, we show that basolateral infection/stimulation
300 leads to a higher induction and secretion of IFNλ2/3 compared to an apical
301 infection. We show that the clathrin adaptor AP-1B sorting machinery allows for
302 the asymmetric distribution of TLR3, allowing IECs to be more responsive from
303 their basolateral side. Interference with AP-1B renders IECs more sensitive to
304 apical stimuli. We propose that this polarized immune response represents a
305 unique immune-strategy to create a homeostatic interface between the complex
306 microbial environment of the gut lumen and the intestinal epithelial barrier. It
307 allows IECs to restrain their immune response against the naturally present
308 apical stimuli while remaining fully responsive to infection/stimulation
309 emanating from the physiologically sterile basolateral side, which will only be
310 accessible during loss of barrier function or during infection by invasive
311 pathogens.

312

313 Only a few studies have tried to correlate the specific localization of TLRs
314 at the apical and basolateral side of IECs with their capacity to respond to
315 PAMPs. TLR5 has been shown to be located on the basolateral membrane, which
316 was suggested to be critical to limit overstimulation of IECs by the commensal
317 bacterial components flagellin (Gewirtz et al., 2001). TLR2 and 4 have been
318 described to be redistributed near the basolateral side of IECs upon activation
319 (Cario et al., 2002, Hiemstra et al., 2015). It was suggested that this trafficking is
320 a mechanism used by IECs to transmit information from the lumen into
321 underlying the immune cells (Hiemstra et al., 2015). TLR9 was shown to be
322 located in both the apical and basolateral membranes but has been described to
323 signal in a polarized manner. Basolateral stimulation of TLR9 leads to NFkB
324 activation and the induction of an immune response however, apical stimulation
325 leads to the ubiquitination of IkBa which causes it to accumulate therefore
326 blocking apical signaling (Lee et al., 2006). Together with the current work on
327 TLR3, the asymmetric distribution of TLRs in IECs appears to represent a
328 mechanism to avoid/control response against lumenal stimuli. Interestingly, a
329 new study suggests that to achieve homeostasis, which we define here as co-
330 habitation of IECs with the commensal flora, TLRs are differentially localized to
331 specific sections in the GI tract (Price et al., 2018). Compatible to the present
332 study, TLR2, 4, and 5 were found at both the apical and basolateral membranes.
333 Interestingly, this study also showed that TLR7 and 9 were absent from the
334 epithelium and their expression was limited to underlying immune cells. Our
335 findings are consistent with this work as we also measured very low expression
336 levels of TLR7/9 and observed that IECs are not responsive to the corresponding
337 agonists. TLR3 was found to be expressed in all intestinal sections (Price et al.,

338 2018, Pott et al., 2012, Cario and Podolsky, 2000). We show that TLR3 is
339 specifically localized at the basolateral side of IECs providing these cells the
340 possibility of mounting a polarized immune response. We could demonstrate
341 that TLR3 displays a polarized functionality independently of its location within
342 the GI tract. We found that basolateral infection leads to a stronger immune
343 response in organoids derived from duodenum, ileum and colon (data not
344 shown). Together these studies suggest that to achieve homeostasis, TLRs
345 expression has to be spatially controlled both at the cellular level
346 (apical/basolateral) and at the longitudinal level along the GI tract.
347
348 We report that AP-1B is responsible for targeting TLR3 to the basolateral
349 side of IECs. The function of clathrin adapter proteins in participating in the
350 regulation of TLR-mediated signaling was previously suggested. Adapter protein
351 AP-3, has been shown to be critical for TLR4 and TLR7/9 mediated signaling
352 (Mantegazza et al., 2012, Blasius et al., 2010). In the absence of AP-3, TLR7/9 are
353 unable to produce type I IFN and TLR4's recruitment and signaling from
354 phagosomes is impaired. Additionally, AP-1 sigma1c mutations have been found
355 in patients that exhibit a severe auto inflammatory skin disorder and it is
356 suggested that this is due to misregulation of the TLR3 receptor further
357 supporting our model of a key role for AP-1 in TLR3 signaling (Setta-Kaffetzi et
358 al., 2014).
359 Due to the challenge associated with the commensal
360 microbiota/epithelium interface, IECs finely tune their intrinsic immune system.
361 Regulation can be found at the quantitative level by selecting the expression of a
362 subset of TLRs or can be achieved by creating a uniquely tailored response that

363 allows for directional partial tolerance of PAMPs. We propose that in addition to
364 plasma membrane-associated TLRs, IECs also functionally polarize the
365 intracellular endosomal TLR3. This polarization of function is intrinsically linked
366 to the polarized nature of the cell and allows for TLR3 to strongly respond to
367 basolateral challenges while limiting response to apical challenges (Sup. Figure
368 12). A recent study has shown that production of a type III interferon mediated
369 antiviral immune response in mice was key to protect them from subsequent
370 enteric virus infections (Ingle et al., 2019). This suggests that production of type
371 III IFN against enteric viruses is key to protecting the gut against further
372 challenges. In the context of our polarized immune response to viral infection,
373 we propose that apical infection/challenges create a sufficient immune response
374 allowing the non-infected bystander cells to be primed for further challenges. If
375 this primed antiviral state is overruled by viruses, upon spreading and infection
376 of IECs from their basolateral side, a stronger immune response will be
377 generated acting as a second line of defense against the pathogen. Importantly,
378 AP-1B knock-out mice show an increase in inflammation and infiltration of CD4+
379 T cells due to an overreaction of IECs against the commensal flora (Takahashi et
380 al., 2011). In the line with our results that AP-1B functionally polarizes PRR
381 sensing and signaling, we propose that within the physiological organization of
382 the gut, this side specific polarized immune response of IECs participates in the
383 tolerance of the commensal flora located in the lumen while remaining
384 responsive to invading pathogens that will gain access to the sterile basolateral
385 side.

Acknowledgments

This work was supported by a research grant from Chica and Heinz Schaller Foundation and Deutsche Forschungsgemeinschaft (DFG) (Project number 240245660 (Project 14 of SFB 1129) and 278001972 (Project A09 of TRR186) to SB). This project has received funding from the European Union's Seventh Framework Programme under grant agreement no 334336 (FP7-PEOPLE-2012-CIG). MS was supported by the Olympia Morata Fellowship from Heidelberg University Hospital, the Brigitte-Schlieben Lange Program from the state of Baden Württemberg, Germany and the Dual Career Support from CellNetworks, Heidelberg, Germany. MM is supported by the TRR186. KP and SM were supported by the SFB1129.

Author Contributions

SB[a]=Steeve Boulant , SB[b]=Sina Bartfeld

MLS and SB[a] designed experiments, MLS, SM, KP, MM and DA performed experiments, MLS analyzed data, TH analyzed microarray data, TK and HO generated the KO mice organoids, CO and JK assisted in establishing polarized infection. SB[b] designed and performed microinjection, VH assisted for the polarized sorting, MLS and SB[a] wrote the manuscript. The final version of the manuscript was approved by all authors.

Declaration of Interests

The authors declare no competing interests.

411 **References**

412 ARPAIA, N. & BARTON, G. M. 2011. Toll-like receptors: key players in antiviral
413 immunity. *Curr Opin Virol,* 1**,** 447-54.
414 BARTFELD, S. & CLEVERS, H. 2015. Organoids as Model for Infectious Diseases:
415 Culture of Human and Murine Stomach Organoids and Microinjection of
416 Helicobacter Pylori. *J Vis Exp*.
417 BARTON, G. M. & MEDZHITOV, R. 2003. Toll-like receptor signaling pathways.
418 *Science,* 300**,** 1524-5.
419 BLASIUS, A. L., ARNOLD, C. N., GEORGEL, P., RUTSCHMANN, S., XIA, Y., LIN, P.,
420 ROSS, C., LI, X., SMART, N. G. & BEUTLER, B. 2010. Slc15a4, AP-3, and
421 Hermansky-Pudlak syndrome proteins are required for Toll-like receptor
422 signaling in plasmacytoid dendritic cells. *Proc Natl Acad Sci U S A,* 107**,**
423 19973-8.
424 BOULANT, S., STANIFER, M., KURAL, C., CURETON, D. K., MASSOL, R., NIBERT, M.
425 L. & KIRCHHAUSEN, T. 2013. Similar uptake but different trafficking and
426 escape routes of reovirus virions and infectious subvirion particles
427 imaged in polarized Madin-Darby canine kidney cells. *Mol Biol Cell,* 24**,**
428 1196-207.
429 BROERING, T. J., MCCUTCHEON, A. M., CENTONZE, V. E. & NIBERT, M. L. 2000.
430 Reovirus nonstructural protein muNS binds to core particles but does not
431 inhibit their transcription and capping activities. *J Virol,* 74**,** 5516-24.
432 CARIO, E., BROWN, D., MCKEE, M., LYNCH-DEVANEY, K., GERKEN, G. &
433 PODOLSKY, D. K. 2002. Commensal-associated molecular patterns induce
434 selective toll-like receptor-trafficking from apical membrane to
435 cytoplasmic compartments in polarized intestinal epithelium. *Am J Pathol,*
436 160**,** 165-73.
437 CARIO, E. & PODOLSKY, D. K. 2000. Differential alteration in intestinal epithelial
438 cell expression of toll-like receptor 3 (TLR3) and TLR4 in inflammatory
439 bowel disease. *Infect Immun,* 68**,** 7010-7.
440 CHASSAING, B., LEY, R. E. & GEWIRTZ, A. T. 2014. Intestinal epithelial cell toll-
441 like receptor 5 regulates the intestinal microbiota to prevent low-grade
442 inflammation and metabolic syndrome in mice. *Gastroenterology,* 147**,**
443 1363-77 e17.
444 CHOW, J., FRANZ, K. M. & KAGAN, J. C. 2015. PRRs are watching you: Localization
445 of innate sensing and signaling regulators. *Virology,* 479-480**,** 104-9.
446 FOLSCH, H. 2015. Role of the epithelial cell-specific clathrin adaptor complex AP-
447 1B in cell polarity. *Cell Logist,* 5**,** e1074331.
448 FUKATA, M. & ARDITI, M. 2013. The role of pattern recognition receptors in
449 intestinal inflammation. *Mucosal Immunol,* 6**,** 451-63.
450 GEWIRTZ, A. T., NAVAS, T. A., LYONS, S., GODOWSKI, P. J. & MADARA, J. L. 2001.
451 Cutting edge: bacterial flagellin activates basolaterally expressed TLR5 to
452 induce epithelial proinflammatory gene expression. *J Immunol,* 167**,** 1882-
453 5.
454 HIEMSTRA, I. H., VRIJLAND, K., HOGENBOOM, M. M., BOUMA, G., KRAAL, G. &
455 DEN HAAN, J. M. 2015. Intestinal epithelial cell transported TLR2 ligand
456 stimulates Ly6C(+) monocyte differentiation in a G-CSF dependent
457 manner. *Immunobiology,* 220**,** 1255-65.

458 INGLE, H., LEE, S., AI, T., ORVEDAHL, A., RODGERS, R., ZHAO, G., SULLENDER, M.,
459 PETERSON, S. T., LOCKE, M., LIU, T. C., YOKOYAMA, C. C., SHARP, B.,
460 SCHULTZ-CHERRY, S., MINER, J. J. & BALDRIDGE, M. T. 2019. Viral
461 complementation of immunodeficiency confers protection against enteric
462 pathogens via interferon-lambda. *Nat Microbiol*.
463 KAGAN, J. C. & BARTON, G. M. 2014. Emerging principles governing signal
464 transduction by pattern-recognition receptors. *Cold Spring Harb Perspect*
465 *Biol,* 7**,** a016253.
466 KANAYA, T., SAKAKIBARA, S., JINNOHARA, T., HACHISUKA, M., TACHIBANA, N.,
467 HIDANO, S., KOBAYASHI, T., KIMURA, S., IWANAGA, T., NAKAGAWA, T.,
468 KATSUNO, T., KATO, N., AKIYAMA, T., SATO, T., WILLIAMS, I. R. & OHNO,
469 H. 2018. Development of intestinal M cells and follicle-associated
470 epithelium is regulated by TRAF6-mediated NF-kappaB signaling. *J Exp*
471 *Med,* 215**,** 501-519.
472 LE BIVIC, A., REAL, F. X. & RODRIGUEZ-BOULAN, E. 1989. Vectorial targeting of
473 apical and basolateral plasma membrane proteins in a human
474 adenocarcinoma epithelial cell line. *Proc Natl Acad Sci U S A,* 86**,** 9313-7.
475 LEE, J., MO, J. H., KATAKURA, K., ALKALAY, I., RUCKER, A. N., LIU, Y. T., LEE, H. K.,
476 SHEN, C., COJOCARU, G., SHENOUDA, S., KAGNOFF, M., ECKMANN, L., BEN-
477 NERIAH, Y. & RAZ, E. 2006. Maintenance of colonic homeostasis by
478 distinctive apical TLR9 signalling in intestinal epithelial cells. *Nat Cell Biol,*
479 8**,** 1327-36.
480 MADARA, J. L., STAFFORD, J., DHARMSATHAPHORN, K. & CARLSON, S. 1987.
481 Structural analysis of a human intestinal epithelial cell line.
482 *Gastroenterology,* 92**,** 1133-45.
483 MANTEGAZZA, A. R., GUTTENTAG, S. H., EL-BENNA, J., SASAI, M., IWASAKI, A.,
484 SHEN, H., LAUFER, T. M. & MARKS, M. S. 2012. Adaptor protein-3 in
485 dendritic cells facilitates phagosomal toll-like receptor signaling and
486 antigen presentation to CD4(+) T cells. *Immunity,* 36**,** 782-94.
487 ODENDALL, C. & KAGAN, J. C. 2017. Activation and pathogenic manipulation of
488 the sensors of the innate immune system. *Microbes Infect,* 19**,** 229-237.
489 PETERSON, L. W. & ARTIS, D. 2014. Intestinal epithelial cells: regulators of
490 barrier function and immune homeostasis. *Nat Rev Immunol,* 14**,** 141-53.
491 POTT, J. & HORNEF, M. 2012. Innate immune signalling at the intestinal
492 epithelium in homeostasis and disease. *EMBO Rep,* 13**,** 684-98.
493 POTT, J., STOCKINGER, S., TOROW, N., SMOCZEK, A., LINDNER, C., MCINERNEY,
494 G., BACKHED, F., BAUMANN, U., PABST, O., BLEICH, A. & HORNEF, M. W.
495 2012. Age-dependent TLR3 expression of the intestinal epithelium
496 contributes to rotavirus susceptibility. *PLoS Pathog,* 8**,** e1002670.
497 PRICE, A. E., SHAMARDANI, K., LUGO, K. A., DEGUINE, J., ROBERTS, A. W., LEE, B.
498 L. & BARTON, G. M. 2018. A Map of Toll-like Receptor Expression in the
499 Intestinal Epithelium Reveals Distinct Spatial, Cell Type-Specific, and
500 Temporal Patterns. *Immunity,* 49**,** 560-575 e6.
501 RITCHIE, M. E., PHIPSON, B., WU, D., HU, Y., LAW, C. W., SHI, W. & SMYTH, G. K.
502 2015. limma powers differential expression analyses for RNA-sequencing
503 and microarray studies. *Nucleic Acids Res,* 43**,** e47.
504 RODRIGUEZ-BOULAN, E. & MACARA, I. G. 2014. Organization and execution of
505 the epithelial polarity programme. *Nat Rev Mol Cell Biol,* 15**,** 225-42.

506 SETTA-KAFFETZI, N., SIMPSON, M. A., NAVARINI, A. A., PATEL, V. M., LU, H. C.,
507 ALLEN, M. H., DUCKWORTH, M., BACHELEZ, H., BURDEN, A. D., CHOON, S.
508 E., GRIFFITHS, C. E., KIRBY, B., KOLIOS, A., SEYGER, M. M., PRINS, C.,
509 SMAHI, A., TREMBATH, R. C., FRATERNALI, F., SMITH, C. H., BARKER, J. N.
510 & CAPON, F. 2014. AP1S3 mutations are associated with pustular
511 psoriasis and impaired Toll-like receptor 3 trafficking. *Am J Hum Genet,*
512 94**,** 790-7.
513 SHAH, P. N. M., STANIFER, M. L., HOHN, K., ENGEL, U., HASELMANN, U.,
514 BARTENSCHLAGER, R., KRAUSSLICH, H. G., KRIJNSE-LOCKER, J. &
515 BOULANT, S. 2017. Genome packaging of reovirus is mediated by the
516 scaffolding property of the microtubule network. *Cell Microbiol,* 19.
517 SHI, W., OSHLACK, A. & SMYTH, G. K. 2010. Optimizing the noise versus bias
518 trade-off for Illumina whole genome expression BeadChips. *Nucleic Acids*
519 *Res,* 38**,** e204.
520 SMYTH, G. K. 2004. Linear models and empirical bayes methods for assessing
521 differential expression in microarray experiments. *Stat Appl Genet Mol*
522 *Biol,* 3**,** Article3.
523 STANIFER, M. L., RIPPERT, A., KAZAKOV, A., WILLEMSEN, J., BUCHER, D.,
524 BENDER, S., BARTENSCHLAGER, R., BINDER, M. & BOULANT, S. 2016.
525 Reovirus intermediate subviral particles constitute a strategy to infect
526 intestinal epithelial cells by exploiting TGF-beta dependent pro-survival
527 signaling. *Cell Microbiol,* 18**,** 1831-1845.
528 STURZENBECKER, L. J., NIBERT, M., FURLONG, D. & FIELDS, B. N. 1987.
529 Intracellular digestion of reovirus particles requires a low pH and is an
530 essential step in the viral infectious cycle. *J Virol,* 61**,** 2351-61.
531 TAKAHASHI, D., HASE, K., KIMURA, S., NAKATSU, F., OHMAE, M., MANDAI, Y.,
532 SATO, T., DATE, Y., EBISAWA, M., KATO, T., OBATA, Y., FUKUDA, S.,
533 KAWAMURA, Y. I., DOHI, T., KATSUNO, T., YOKOSUKA, O., WAGURI, S. &
534 OHNO, H. 2011. The epithelia-specific membrane trafficking factor AP-1B
535 controls gut immune homeostasis in mice. *Gastroenterology,* 141**,** 621-32.
536 YAMAMOTO, M., SATO, S., HEMMI, H., HOSHINO, K., KAISHO, T., SANJO, H.,
537 TAKEUCHI, O., SUGIYAMA, M., OKABE, M., TAKEDA, K. & AKIRA, S. 2003.
538 Role of adaptor TRIF in the MyD88-independent toll-like receptor
539 signaling pathway. *Science,* 301**,** 640-3.
540 YU, S. & GAO, N. 2015. Compartmentalizing intestinal epithelial cell toll-like
541 receptors for immune surveillance. *Cell Mol Life Sci,* 72**,** 3343-53.
542
543

544 **Figure Legends:**

545

546 **Figure 1. T84 cells respond to TLR3 agonist in a side-specific manner.** (A).
547 The relative expression of TLR2-9 was evaluated in T84 cells by q-RT-PCR.
548 Results are expressed as a relative expression to the house-keeping gene HPRT1.
549 (B) Diagram depicting the side specific stimulation (apical vs. basolateral) of
550 polarized T84 cells grown on transwells by TLR agonists. (C) T84 cells were
551 seeded on transwells and after establishment of barrier function, cells were
552 treated with the following TLR agonists: TLR1/2 (PAM3CSK4, 1 μg/mL); TLR3
553 (1:1 HMW and LMW poly I:C, 10 μg/mL); TLR4 (LPS-EK, 0.01 μg/mL); TLR5
554 (Flagellin-ST, 1 μg/mL); TLR7/8 (R848, 1 μg/mL), TLR9 (ODN 2395 5 μM). 6
555 hours post-treatment, RNA was harvested and evaluated for the up-regulation of
556 IL-6 by q-RT-PCR. Results are normalized to mock-treated samples. (D) Same as
557 C except type III IFN (IFNλ2/3) was measured. (E) T84 cells were seeded on
558 transwells and treated with 10 μg/mL of poly I:C. Cells were harvested at the
559 indicated time points and up-regulation of both type I (IFNβ) and type III
560 (IFNλ2/3) IFNs were analyzed by q-RT-PCR. Experiments were performed in
561 triplicate, error bars indicate the standard deviation. ns=not significant, *<P.05
562 (unpaired t-test)

563

564 **Figure 2. Intrinsic immune response of T84 cells to viral infection is side**
565 **specific.** T84 cells were seeded onto transwell inserts and allowed to establish
566 barrier function. (A) Schematic depicting infection of T84 cells in a side specific
567 manner. (B) Polarized T84 cells were infected apically or basolaterally with

568 mammalian reovirus (MRV). 16 hours post-infection (hpi) cells were fixed and
569 indirect immunofluorescence was performed to control the integrity of the tight
570 junction belt (tight junction protein ZO-1, red) and to evaluate the viral non-
571 structural protein μNS (green). Nuclei were visualized with DAPI. (C) Polarized
572 T84 cells were infected apically or basolaterally with MRV. At indicated time
573 points, cells were fixed and stained for the viral non-structural protein μNS. The
574 number of infected cells was counted in ten independent fields of view for each
575 sample. (D) Polarized T84 cells were infected apically or basolaterally with MRV.
576 At indicated time points cells were harvested and Western blot was used to
577 detect the amount of the non-structural protein μNS in each sample (left panel).
578 The relative amount of μNS normalized to actin was quantified for each time
579 point post-infection (right panel). (E) Same as D except cells were lysed and
580 production of progeny viruses was evaluated using a plaque assay. (F-G)
581 Polarized T84 cells were infected apically or basolaterally with MRV. 16 hpi, cells
582 were harvested and the production of interferons was analyzed by q-RT-PCR. (F)
583 Type I (IFNβ). (G) Type III (IFNλ2/3). (H) Same as G except that production of
584 type III (IFNλ2/3) IFN was analyzed by ELISA. Experiments were performed in
585 triplicate, representative images for Western blot and immunofluorescence are
586 shown, error bars indicate the standard deviation. ns=not significant, *<P.05, **P
587 < 0.01 (unpaired t-test)
588
589 **Figure 3. Human organoids respond in a polarized manner to TLR3 agonist.**
590 (A) Human organoids were seeded onto transwells and allowed to polarize and
591 differentiate for five days (see method for details). Polarized monolayers were
592 infected with MRV apically or basolaterally and assessed 16 hpi for (B) viral

593 infection by indirect immunofluorescence (green=μNS, red=ZO-1, blue=DAPI)
594 and (C) for the amount of viral genome present. (D) The production of both type
595 I (IFNβ) and type III (IFNλ2/3) interferons was evaluated by q-RT-PCR. (E) Same
596 as D except type III IFN secretion was quantified by ELISA. (F) Colon organoids
597 were seeded on transwells and treated with the indicated TLR agonist. TLR1/2
598 (PAM3CSK4, 1 μg/mL); TLR3 (1:1 HMW and LMW poly I:C, 10 μg/mL); TLR4
599 (LPS-EK, 0.01 μg/mL); TLR5 (Flagellin-ST, 1 μg/mL); TLR7/8 (R848, 1 μg/mL),
600 TLR9 (ODN 2395 5 μM). 6 hours post-treatment RNA was harvested and
601 evaluated for the up-regulation of IL-6 by q-RT-PCR. Results are normalized to
602 mock-treated samples. (G) Same as F, except type III IFN (IFNλ2/3) was
603 evaluated. All experiments were performed in triplicate. Representative
604 immunofluorescence images are shown. Error bars indicate the standard
605 deviation. Scale bar in (B) represents 10 μm. ns=not significant, *<P.05, **P <
606 0.01 (unpaired t-test).
607
608 **Figure 4. TLR3 is localized to the basolateral side of intestinal epithelial**
609 **cells.** (A). Human colon organoids were seeded flat on a Labtek chamber pre-
610 coated with Matrigel. Following fixation with PFA, cells were immunostained
611 against TLR3 (red), ZO-1 (green), actin was labeled with phalloidin 647
612 (magenta) and the nuclei were stained with DAPI (blue). (B) Schematic depicting
613 a T84-derived spheroid or a small organoid, with the apical membrane of hIECs
614 facing the lumen of the structure and their basolateral membrane facing
615 outward. (C) Human colon organoids and T84-derived spheroids were
616 immunostained against TLR3 (green), ZO-1 (red), actin was labeled with

617 phalloidin 647 (magenta) and the nuclei were stained with DAPI (blue). (D) The
618 percentage of spheroids displaying TLR3 at the apical or basolateral membrane
619 of hIECs was quantified (For organoids n=51, for T84 cells n=84). Experiments
620 were performed in triplicate, representative images are shown. Scale bar
621 represents 20 μm.
622
623 **Figure 5. The clathrin sorting adaptor AP-1B is responsible for the**
624 **basolateral localization of TLR3 in hIECs.** (A) WT and AP-1B knock-down T84
625 spheroids were immunostained against TLR3 (green), ZO-1 (red), actin was
626 labeled with phalloidin 647 (magenta) and the nuclei were stained with DAPI
627 (blue). (B) Same as A except cells were immunostained for Laminin (red) as a
628 basolateral marker. (C) Quantification of the localization of TLR3 in WT and AP-
629 1B knock-down T84 spheroids. The relative fluorescence intensity of TLR3 is
630 depicted along a transversal line going in the middle of the spheroids. (D) The
631 percentage of spheroids displaying TLR3 at the apical or basolateral membrane
632 of hIECs was quantified. (for WT spheroids n=84, for AP-1B knock-down T84
633 spheroids n=111). Experiments were performed in triplicate, representative
634 images are shown. Scale bar represents 20 μm.
635
636 **Figure 6. The clathrin sorting adaptor AP-1B is responsible for the TLR3-**
637 **mediated polarized immune response.** (A) WT and AP-1B knock-down T84
638 cells were polarized on transwell inserts. Cells were infected with MRV apically
639 or basolaterally. At indicated time points, the production of type III (IFNλ2/3)
640 interferon was evaluated by q-RT-PCR. (B) Same as A except polarized T84 cells
641 were stimulated with the TLR3 agonist poly I:C (10 μg/mL). (C) Schematic for

642 the generation of the inducible murine AP-1B knock-out organoids from the
643 Villin-CreER Ap1m2 $^{flox/flox}$ mice. (D). AP-1B knock-out was confirmed by q-RT-
644 PCR for exon 4-5 of the Ap1m2 locus. (E) Non-tamoxifen treated Villin-CreER
645 Ap1m2 $^{flox/flox}$ mice (AP-1B+/+) and tamoxifen treated Villin-CreER Ap1m2 $^{flox/flox}$
646 mice (AP-1B -/-) derived organoids were seeded onto transwells and infected
647 with MRV in a polarized manner. 48 hpi, cells were harvested and analyzed for
648 the induction of IFNλ2/3 by q-RT-PCR. (F) Same as E, except IFNλ2/3 was
649 analyzed by ELISA. (G) Non-tamoxifen treated Villin-CreER Ap1m2 $^{flox/flox}$ mice
650 (AP-1B+/+) and tamoxifen treated Villin-CreER Ap1m2 $^{flox/flox}$ mice (AP-1B -/-)
651 derived organoids were seeded onto transwells and stimulated with the TLR3
652 agonist poly I:C (10 μg/mL). 8 hours post-stimulation, cells were harvested and
653 analyzed for the induction of IL-6 by q-RT-PCR (H) Same as G, except IFNλ2/3
654 was analyzed. All experiments were performed in triplicate. Error bars indicate
655 the standard deviation. ns=not significant, *<P.05, **P < 0.01 (unpaired t-test).
656
657

658 **Materials and Methods**

659 **Cell and Viruses.** T84 human colon carcinoma cells (ATCC CCL-248) were
660 maintained in a 50:50 mixture of Dulbecco's modified Eagle's medium (DMEM)
661 and F12 (GibCo) supplemented with 10% fetal bovine serum and 1%
662 penicillin/streptomycin (Gibco). Mammalian reovirus (MRV) strains Type 3
663 clone 9 (T3C9) derived from stocks originally obtained from Bernard N. Fields
664 were grown and purified by standard protocols (Sturzenbecker et al., 1987).

665

666 **Antibodies and Inhibitors.** Rabbit polyclonal antibody against MRV μNS was
667 used at 1/1000 for immunostaining and western blots (Broering et al., 2000,
668 Shah et al., 2017); ZO-1 (mouse from Santa Cruz Biotechnology and rabbit from
669 Thermo Scientific) were both used at 1/100 for immunostaining; actin (Sigma-
670 Aldrich) was used at 1/2000 for western blots; Phalloidin-AF647 (Molecular
671 Probes) was used at 1/200 for immunostaining; Laminin (Abcam) was used at
672 1/100 for immunostaining, and TLR3 (Abcam) was used at 1/100 for
673 immunostaining. Secondary antibodies were conjugated with AF488 (Molecular
674 Probes), AF568 (Molecular Probes), AF647 (Molecular Probes), CW800 (Li-Cor)
675 or HRP (Sigma-Aldrich) directed against the animal source. TRIF peptide
676 inhibitor was used at a final concentration of 25 μM (Invivogen). Actinomycin D
677 (Sigma) was used at a final concentration of 4 μg/mL. TLR stimuli: Flagellin-ST
678 (InivoGen), ODN 2395, 2006, and 2243 (InvivoGen), LPS-EK (InvivoGen), poly I:C
679 (Invivogen), poly I:C HMW Fluorescein (InvivoGen), Pam3CSK4 (InvivoGen) and
680 R848 (InvivoGen) were used at the concentrations listed in figure legends.

681

682 **Viral infections.** All MRV infections were performed at a MOI of 1. Media was
683 removed from transwells and virus containing media was added to either the
684 apical or basolateral side. Virus was maintained for the course of the experiment.
685
686 **Polarization of T84 cells on transwell inserts.** $1.2x10^5$ T84 cells were seeded
687 on polycarbonate transwell inserts (Corning, polycarbonate, 3.0 μM) in
688 DMEM/F12 medium. Medium was replaced 24h post-seeding and every two
689 days subsequently. The trans-epithelial electrical resistance (TEER) was tested
690 as indicated with $EVOM^2$ apparatus (World Precision Instrument). When the
691 TEER reached 1000 Ohm/cm^2, the T84 cells were considered polarized (Madara
692 et al., 1987). Polarization was controlled by immunostaining of the tight junction
693 protein ZO-1 (see indirect immunofluorescence assay).
694
695 **Seeding of T84 cells into spheroids.** T84 cells were dissociated using 0.25%
696 trypsin, washed with PBS and resuspended in culture medium containing 4%
697 Matrigel. Dissociated cells were seeded into Matrigel-coated eight-well chamber
698 slides (Lab-Tek, eight-well chamber slides, Nunc, 155411) at a concentration of
699 12,000 single cells per well. Chamber slides were coated with 10 μl pure Matrigel
700 and incubated at 37°C for 2 min before cell seeding. Cells were incubated for six
701 days and fixed using 2% PFA for 20 min. Immunostaining of spheroids was
702 carried out as described below.
703
704 **RNA isolation, cDNA, and qPCR.** RNA was harvested from cells using
705 NuceloSpin RNA extraction kit (Machery-Nagel) as per manufactures
706 instructions. cDNA was made using iSCRIPT reverse transcriptase (BioRad) from

707 250 ng of total RNA as per manufactures instructions. q-RT-PCR was performed
708 using SsoAdvanced SYBR green (BioRad) as per manufacturer's instructions, TBP
709 and HPRT1 were used as normalizing genes. For mouse interferon lambda and
710 HPRT1 TaqMan gene expression assays were used.
711
712 **Indirect Immunofluorescence Assay.** Polycarbonate transwell inserts were cut
713 in half or cells were fixed in 2% paraformaldehyde (PFA) for 20 mins at room
714 temperature (RT). Cells were washed and permeabilized in 0.5% Triton-X for 15
715 mins at RT. Primary antibodies were diluted in phosphate-buffered saline (PBS)
716 and incubated for 1h at RT. Membranes were washed in 1X PBS three times and
717 incubated with secondary antibodies for 45 mins at RT. Membranes were
718 washed in 1X PBS three times and mounted on slides with ProLong Gold DAPI
719 (Molecular Probes). Cells were imaged by epifluorescence on a Nikon Eclipse Ti-
720 S (Nikon) or by confocal tile scans on a Zeiss LSM 780 (Zeiss). ZO-1 images were
721 acquired on an ERS 6 spinning disc confocal microscope and deconvolution was
722 performed using Huygens Remote Manager. Spheroids and 3D organoids were
723 imaged on an inverted spinning disc confocal microscope (Nikon, PerkinElmer)
724 with 60x (1.2 numerical aperture, PlanApo, Nikon) water immersion objective
725 and an EMCCD camera (Hamamatsu C9100-23B).
726
727 **Western blot.** At time of harvest, media was removed, cells were rinsed one
728 time with 1X PBS and lysed with 1X RIPA (150 mM sodium chloride, 1.0% Triton
729 X-100, 0.5% sodium deoxycholate, 0.1% sodium dodecyl sulphate (SDS), 50 mM
730 Tris, pH 8.0 with phosphatase and protease inhibitors (Sigma-Aldrich)) for 5
731 mins at RT. Lysates were collected and equal protein amounts were separated by

732 SDS-PAGE and blotted onto a nitrocellulose membrane by wet-blotting (Bio-Rad,
733 Germany). Membranes were blocked with 5% milk or 5% BSA in TBS containing
734 0.1% Tween 20 (TBS-T) for one hour at room temperature. Primary antibodies
735 were diluted in blocking buffer and incubated overnight at 4°C. Membranes were
736 washed 3X in TBS-T for 5 mins at RT. Secondary antibodies were diluted in
737 blocking buffer and incubated at RT for 1 h with rocking. For film exposure:
738 membranes were washed 3X in TBS-T for 5 mins at RT. HRP detection reagent
739 (GE Healthcare) was mixed 1:1 and incubated at RT for 5mins. Membranes were
740 exposed to film and developed. For LiCOR assays, membranes were scanned on a
741 LiCOR Odyssey imager.
742
743 **ELISA:** Supernatants were collected at time points indicated in figure legends.
744 Supernatants were kept undiluted. IFNλ2/3 was evaluated using the IFNλ2/3
745 DIY ELISA (PBL Interferon source) for the basolateral supernatants only as we
746 have previously shown that IFNλ is preferentially secreted to the basolateral
747 compartment (Stanifer et al., 2016). IL-6 was evaluated using the IL-6 DIY ELISA
748 (Biolegend). ELISA was performed as per manufacturers instructions.
749
750 **Plaque Assay.** BSC-1 were seeded into 24-well plates at a density of
751 200,000cells/well. 24-48h post-seeding when cells had reached 100%
752 confluency, media was removed and cells were washed 1X with PBS+2mM $MgCl_2$
753 (PBS-M). Virus samples were harvested from infected T84 cells and were subject
754 to three rounds of freezing and thawing. Samples were spun to remove cellular
755 debris and virus containing supernatants were diluted in 10-fold serial dilutions
756 in PBS-M. Infection was allowed to proceed for 1h at RT with rocking every 15

757 mins. At the end of the incubation time, cells were overlaid with a 1:1 mixture of
758 2% agarose:2X 199 Media (Sigma-Aldrich) containing 10 μg/mL chymotrypsin.
759 Cells were incubated at 37°C for 48h or until the appearance of plaques. Cells
760 were fixed in 10% formaldehyde for 30 mins at RT. Plugs were removed and
761 cells were stained with 0.5% crystal violet for 15 mins at RT. Crystal violet was
762 removed and cells were washed with water. Plaques were counted and all
763 samples were performed in triplicate.
764
765 **Fluorescent poly I:C uptake assay.** 1 x 10^5 T84 cells were grown on collagen
766 coated transwell filters until reaching full polarization. HMW poly I:C fluorescein
767 was added to the apical or basolateral surface at a concentration of 10 μg/mL.
768 After incubating at 37°C for the indicated time points, transwells were washed
769 with PBS and then incubated with an acid wash (PBS, 0.2M acetic acid, 0.5M
770 NaCl) for 10 sec to remove any non-internalized poly IC. Cells were then washed
771 three times in 1X PBS followed by lysis in RIPA buffer. The amount of
772 fluorescence of the internalized virus was measured on a Tecan infinite M200
773 Pro at 495 nm. Cells which were not fed poly IC or where poly IC was added and
774 immediately removed were used as a background control.
775
776 **Dextran uptake assay.** 1 x 10^5 T84 cells were grown on collagen coated
777 transwell filters. At the indicated time, the diffusion of FITC-labelled dextran was
778 measured. FITC-labeled dextran (Sigma-Aldrich, 4 kDa) was to the apical surface
779 at a final concentration of 2 mg/mL. After incubating for 3 h 37°C, 100 μL
780 aliquots of the basal media were collected and the fluorescence was measured
781 with the FLUOstar Omega spectrofluorometer (BMG Labtech) at 495 nm. As

782 positive control, fluorescence of 100 µL aliquot of a collagen coated but cell-free
783 transwell filter was measured to assess maximum diffusion of FITC-labeled
784 dextran.
785
786 **Fluorescent viral uptake assay.** 1 x 10^5 T84 cells were grown on collagen
787 coated transwell filters until reaching 1000Ω/cm^2. AF488-labelled MRV (Boulant
788 et al., 2013) was to the apical or basolateral surface at a MOI=1. After incubating
789 at 37°C for the indicated time points, transwells were washed with PBS and then
790 incubated with an acid wash (PBS, 0.2M acetic acid, 0.5M NaCl) for 10 sec to
791 remove any non-internalized virus particle. Cells were then washed three times
792 in 1X PBS followed by lysis in RIPA buffer. The amount of fluorescence of the
793 internalized virus was then measured on a Tecan infinite M200 Pro at 495 nm.
794 Cells which were not infected with virus or were virus was added and
795 immediately removed were used as a background control.
796
797 **Human organoid cultures.** Human tissue was received from colon and small
798 intestine resection from the University Hospital Heidelberg. This study was
799 carried out in accordance with the recommendations of the University hospital
800 Heidelberg with written informed consent from all subjects in accordance with
801 the Declaration of Helsinki. All samples were received and maintained in an
802 anonymized manner. The protocol was approved by the "Ethics commission of
803 the University Hospital Heidelberg" under the protocol S-443/2017. Stem cells
804 containing crypts were isolated following 2 mM EDTA dissociation of tissue
805 sample for 1 h at 4°C. Crypts were spun and washed in ice cold PBS. Fractions
806 enriched in crypts were filtered with 70 µM filters and the fractions were

807 observed under a light microscope. Fractions containing the highest number of
808 crypts were pooled and spun again. The supernatant was removed and crypts
809 were re-suspended in Matrigel. Crypts were passaged and maintained in basal
810 and differentiation culture media (see table 1).
811
812 **Mouse organoids.** Mouse intestinal tissue was received from control floxed
813 mice or mice expressing a floxed Ap1m2 gene as previously described (Kanaya et
814 al., 2018). Organoids were harvested, passaged and maintained in cultures as
815 previously described for the human organoids, except using mouse specific
816 media conditions (see table 1). To obtain organoids lacking the Ap1m2 gene,
817 organoids were treated with 20 μM tamoxifen for 48h. Tamoxifen was removed
818 and cells were allowed to recover and grow in normal mouse media.
819
820 **Microinjection.** Human colon organoids were microinjected adapting a
821 previously published protocol (Bartfeld and Clevers, 2015). Microinjection was
822 carried out in a sterile laminar flow hood (KoJair, Finnland) using a
823 micromanipulator (Narishige) and microinjector (Eppendorf FemtoJet). In each
824 well, 30 organoids were injected. The injection needle was placed either inside
825 the organoid (apical infection), or outside the organoid (basal infection), but
826 both time in similar proximity to the epithelium. Pairs of inside and outside
827 injections were on the same plate.
828
829 **Organoids on transwells.** Tranwells were coated with 2.5% collagen in PBS for
830 1 h prior to organoids seeding. Organoids were collected at a ratio of 100
831 organoids/transwell. Collected organoids were spun at 450g for 5 mins and the

832 supernatant was removed. Organoids were washed 1X with cold PBS and spun at
833 450g for 5 mins. PBS was removed and organoids were digested with 0.5%
834 Trypsin-EDTA (Life technologies) for 5 mins at 37°C. Digestion was stopped by
835 addition of serum containing medium. Organoids were spun at 450g for 5 mins
836 and the supernatant was removed and organoids were re-suspended in normal
837 growth media at a ratio of 100 µL media/well. The PBS/matrigel mixture was
838 removed from the transwells and 100 µL of organoids were added to each well.
839 500 µL of normal organoid media was added to the bottom chambers. 24 hours
840 post-seeding media on both sides of the transwells was changed for
841 differentiation media and the TEER was monitored over five days.
842
843 **RNA decay assay.** T84 cells were seeded onto a 24-well plate at a density of
844 100,000cells/well. 24h post-seeding T84 cells were infected with MRV T3C9. 16
845 hours post-infection, cells were treated with 4 µg/mL actinomycin D and RNA
846 samples were collected at time points indicated in figure legend. RNA was
847 harvested and qPCR as performed as described above.
848
849 **Production of Ap1 knock-down T84 cells.** T84 cells were seeded onto 6-well
850 plates in a density of 500,000cells/well. 24h post-seeding cells were transduced
851 with lentiviruses expressing an shRNA targeted for the Ap1m2 gene (sequence
852 available upon request). 72h post-transduction, lentiviruses were removed and
853 T84 cells were put under antibiotic selection. When all control cells had died,
854 antibiotic selection was removed and T84 cells were allowed to re-grow. Knock-
855 down was confirmed through qPCR.
856

857 **Microarray.** T84 cells were seeded on transwell and were allowed to polarize.
858 Once a TEER value of 1000Ω/cm^2 had been reached, cells were infected from the
859 apical and basolateral membranes with MRV at a MOI=1. 16 hours post-infection
860 RNA was collected and 1 µg of total RNA was used for an Illumina HumanHT-12
861 beadarray analysis. Expression values were quantile-normalized after
862 background correction (Shi et al., 2010) and log2-transformed. Unspecific
863 filtering was performed by discarding probes without significant detection p-
864 value in any sample. Differentially expressed probes between A and Mock as well
865 as between B and Mock were identified using the empirical Bayes approach
866 (Smyth, 2004) based on moderated t-statistics as implemented in the
867 Bioconductor package limma (Ritchie et al., 2015). P-values were adjusted for
868 multiple testing using the Benjamini-Hochberg correction in order to control the
869 false discovery rate. Adjusted p-values below 5% were considered statistically
870 significant. For heatmap display, expression values of significantly up-regulated
871 genes (in A or B) were scaled across samples and hierarchical clustering was
872 performed using euclidean distance and complete linkage. Analyses were carried
873 out using R 3.5 with add-on package pheatmap.
874
875 **Statistics.** Statistical analysis was performed using the GraphPad Prism software
876 package.
877
878
879
880

881 **Supplemental Information**

882 **Supplementary Figure 1. Establishment of barrier function by T84 cells.**
883 T84 cells were seeded onto transwell inserts. (A). The rate of establishment of
884 barrier function was measured by the trans-epithelial electrical resistance
885 (TEER) using a chop stick electrode. TEER greater than 1000 Ohm/cm^2 indicates
886 a tight barrier and is marked with a dashed line. (B). Barrier integrity was
887 assessed by dextran diffusion assay. T84 cells were allowed to grow on
888 transwells and at the indicated time points 4kDa fluorescent FITC-Dextran was
889 added to the apical chamber. Three hours post-incubation, basolateral media
890 was collected and analyzed by fluorometry to assess the amount of dextran
891 which has diffused to the basolateral compartment of the transwells. Experiment
892 were performed in triplicate. Error bars indicate the standard deviation. n.d.=
893 not determined.

894

895 **Supplementary Figure 2. Activation of pBMC by TLR ligands and uptake of**
896 **TLR3 agonist by T84 hIECs.** (A) pBMCs were isolated and treated with 10-fold
897 serial dilutions of the indicated TLR agonists (starting concentrations: TLR1/2
898 (PAM3CSK4, 1 μg/mL); TLR3 (1:1 HMW and LMW poly I:C, 10 μg/mL); TLR4
899 (LPS-EK, 1 μg/mL); TLR5 (Flagellin-ST, 1 μg/mL); TLR7/8 (R848, 1 μg/mL),
900 TLR9 (ODN 2395 5 μM)). Supernatants were harvested 24 hours post-
901 stimulation and were tested for IL-6 by ELISA. (B) Polarized T84 cells were fed
902 FITC-labeled poly I:C in a side specific manner. Cells were harvested at indicated
903 time points, were washed with a quick acid wash to remove any non-internalized
904 poly I:C bound to the cell surface. Following acid wash, cells were lysed and the
905 relative amount of internalized FITC-labeled poly I:C was measured by

906 spectrofluorometry. Experiments were performed in triplicate. Error bars
907 indicate the standard deviation. ns=not significant (unpaired t-test).
908
909 **Supplementary Figure 3. Apical infection of T84 cells by MRV leads to more**
910 ***de novo* virus production compared to basolateral infection.** Polarized T84
911 cells were infected apically or basolaterally with MRV. (A) Fluorescently labeled
912 MRV was added to polarized T84 cells in a side specific manner. Cells were
913 collected at indicated times points and were washed with a quick acid wash to
914 remove any non-internalized virus particles bound to the cell surface. Following
915 acid wash, cells were lysed and the relative amount of internalized virus
916 particles was measured by spectrofluorometry. (B) Infected cells were collected
917 at the indicated time points and viral replication was assayed by q-RT-PCR
918 against the MRV μ2 genome segment. (C) Same as B except virus replication was
919 addressed by Western blot against the MRV non-structural protein μNS. Actin
920 was used as a loading control (left panel). Representative figure is shown. The
921 relative expression of μNS is normalized to actin is shown (right panel). (D)
922 Infected cells were fixed at indicated time points and immunofluorescence was
923 performed against the non-structural protein μNS. The number of infected cells
924 per field of view was counted. 10 fields of view were counted for each time point.
925 (E) Polarized T84 cells were infected apically or basolaterally with MRV. Infected
926 cells were collected at the indicated time points and viral replication was
927 assayed by q-RT-PCR against the MRV μ2 genome segment. Experiments were
928 performed in triplicate, error bars indicate the standard deviation. ns=not
929 significant , *<P.05, **P < 0.01 (unpaired t-test)
930

931 **Supplementary Figure 4. Side specific induction of IFN production upon**
932 **viral infection in the human intestinal epithelial line SKCO15 cells.** SKCO15
933 cells were seeded on transwells. Following establishment of barrier function,
934 cells were infected apically or basolaterally with MRV. (A) 16 hpi, the production
935 of type I (IFNβ) and type III (IFNλ2/3) IFNs was assessed by q-RT-PCR. (B)
936 Efficiency of the primary MRV infection in SKCO15 cells was controlled by
937 immunofluorescence against the non-structural protein μNS (red). Cell nuclei
938 were stained using DAPI (blue). Experiments were performed in triplicate.
939 Representative images for IF are shown. Scale bar =100 μm. Error bars indicate
940 standard deviation. ** $P < 0.01$ (unpaired t-test).
941
942 **Supplementary Figure 5. Basolateral infection of T84 cells leads to a**
943 **stronger production of interferon compared to apical infection.** (A) T84
944 cells were infected apically or basolaterally with MRV. RNA samples were
945 collected at the indicated times post-infection and production of type I (IFNβ)
946 and type III (IFNλ2/3) interferons was measured by q-RT-PCR. (B) T84 cells were
947 infected apically or basolaterally with MRV. Supernatants were collected at the
948 indicated times post-infection and analyzed by ELISA for the secretion of type III
949 (IFNλ2/3) interferon. A=apical infection. B =basolateral infection. Black line
950 indicates the limit of detection. All samples were performed in triplicate. Error
951 bars indicate the standard deviation. ns=not significant, *<P.05, **$P < 0.01$, ***$P <$
952 0.001 (unpaired t-test).
953
954 **Supplementary Figure 6. Stronger immune response observed during**
955 **basolateral infection of hIECs is not due to differences in transcript**

956 **stability.** (A) Polarized T84 cells were infected apically or basolaterally with
957 MRV. 16 hpi cells were treated with actinomycin D to block transcription. RNA
958 samples were collected at the indicated times post-actinomycin treatment. (B)
959 Relative amounts of type I (upper panel) and type III IFN (lower panel)
960 transcripts (normalized to the time of actinomycin treatment) were evaluated by
961 q-RT-PCR (left panel). The half-life of each transcripts was determined (right
962 panel). Experiments were performed in triplicate. Error bars indicate the
963 standard deviation. ns=not significant. *<P.05 (unpaired t-test).
964
965 **Supplementary Figure 7. Basolateral infection of T84 cells by MRV leads to**
966 **the upregulation of many immune related genes.** Polarized T84 cells were
967 infected apically or basolaterally with MRV. 16 hpi, RNA was collected and
968 subjected to microarray analysis. Expression values were quantile-normalized
969 after background correction and log2-transformed. Unspecific filtering was
970 performed by discarding genes with non-significant p-values in any sample. (A)
971 Differentially expressed genes between apical infection and mock infected cells
972 as well as between basolateral infection and mock infected cells were identified
973 using the empirical Bayes approach and are shown in a Venn diagram. (B)
974 Heatmap of expression values of significantly up-regulated genes in apically and
975 basolaterally infected cells were scaled across samples and hierarchical
976 clustering was performed using euclidean distance and complete linkage. (C)
977 KEGG analysis of significantly upregulated genes upon basolateral infection of
978 T84 cells.
979

980 **Supplementary Figure 8. Basolateral infection of human organoids by MRV**
981 **generates a stronger intrinsic immune response compared to apical**
982 **infection.** (A) Schematic of the microinjection approach used to infect organoids
983 specifically from either their apical or basolateral sides. (B-C) Human intestinal
984 organoids were infected by MRV apically or basolaterally through
985 microinjection. Virus infection was assessed 16 hpi for (B) the production of the
986 non-structural viral protein μNS using Western blot analysis and (C) the
987 production of the MRV μ2 genome segment by q-RT-PCR. (D) Generation of
988 intrinsic immune response was assessed by quantifying the production of type I
989 (IFNβ) and type III (IFNλ2/3) IFNs using q-RT-PCR. (E) The relative expression of
990 TLR2-9 was evaluated in human intestinal organoids. Results are expressed as a
991 ratio to the house keeping gene HPRT1. All experiments were performed in
992 triplicate. Representative western blot is shown. Error bars indicate the standard
993 deviation. ns=not significant, *<P.05, **P < 0.01 (unpaired t-test).
994
995 **Supplementary Figure 9. Knock-down of the clathrin adaptor AP-1B**
996 **impacts the polarized immune response.** (A) Knock-down efficiency AP-1B
997 was evaluated by q-RT-PCR. (B-D) The integrity of the barrier function of the AP-
998 1B knock down T84 cells was evaluated by (B) indirect immunofluorescence of
999 the tight junction protein Zo-1 (red), (C) dextran diffusion assay and (D) TEER
1000 measurement.(E) Polarized WT and AP-1B knock-down T84 cells were infected
1001 with MRV in a side specific manner. Supernatants were collected at indicated
1002 time points and subjected to ELISA to monitor the amount of secreted type III
1003 IFNs. All experiments were performed in triplicate. Error bars indicate the
1004 standard deviation. Representative image for immunofluorescence is shown.

1005 Scale bar =100 μm. ns=not significant, ** P < 0.01, **** P < 0.0001 (unpaired t-
1006 test).
1007
1008 **Supplementary Figure 10. Stimulation of AP-1B knock-down T84 cells by**
1009 **TLR agonists.** (A) AP-1B knock-down T84 cells were seeded on transwells and
1010 treated with indicated TLR agonists: TLR1/2 (PAM3CSK4, 1 μg/mL); TLR3 (1:1
1011 HMW and LMW poly I:C, 10 μg/mL); TLR4 (LPS-EK, 0.01 μg/mL); TLR5
1012 (Flagellin-ST, 1 μg/mL); TLR7/8 (R848, 1 μg/mL), TLR9 (ODN 2395 5 μM). 6
1013 hours post-treatment RNA was harvested and evaluated for the upregulation of
1014 IL-6 by q-RT-PCR. Results are normalized to mock-treated samples. (B) Same as
1015 A except type III IFN (IFNλ2/3) was evaluated. Experiments were performed in
1016 triplicate; error bars indicate the standard deviation. ns=not significant, *<P.05
1017 (unpaired t-test)
1018
1019 **Supplementary Figure 11. Inhibition of TRIF interferes with the polarized**
1020 **immune response generated by T84 cells.** WT and AP-1B knock-down T84
1021 cells were seeded on transwell inserts. (A) WT cells were treated with a TRIF
1022 inhibitor or a control peptide. T84 cells were infected with MRV in a side specific
1023 manner. RNA samples were harvested at indicated time points post-MRV
1024 infection and the intrinsic innate immune induction was analyzed by q-RT-PCR
1025 for type III IFN (IFNλ2/3). (B) Same as A, except AP-1B knock-down cells were
1026 evaluated. All experiments were performed in triplicate. Error bars indicate the
1027 standard deviation. ns=not significant, * P < 0.05. ** P < 0.01. Statistics in panel B
1028 are between AP-1B and AP-1B+TRIFi.
1029

1030 **Supplementary Figure 12. The clathrin sorting adaptor protein AP-1**
1031 **localizes TLR3 to the basolateral side of hIECs leading to an asymmetric**
1032 **IFN-mediated immune response.** Schematic showing TLR3 localization in
1033 polarized intestinal epithelial cells and its implication for side specific interferon
1034 induction upon viral infection.
1035

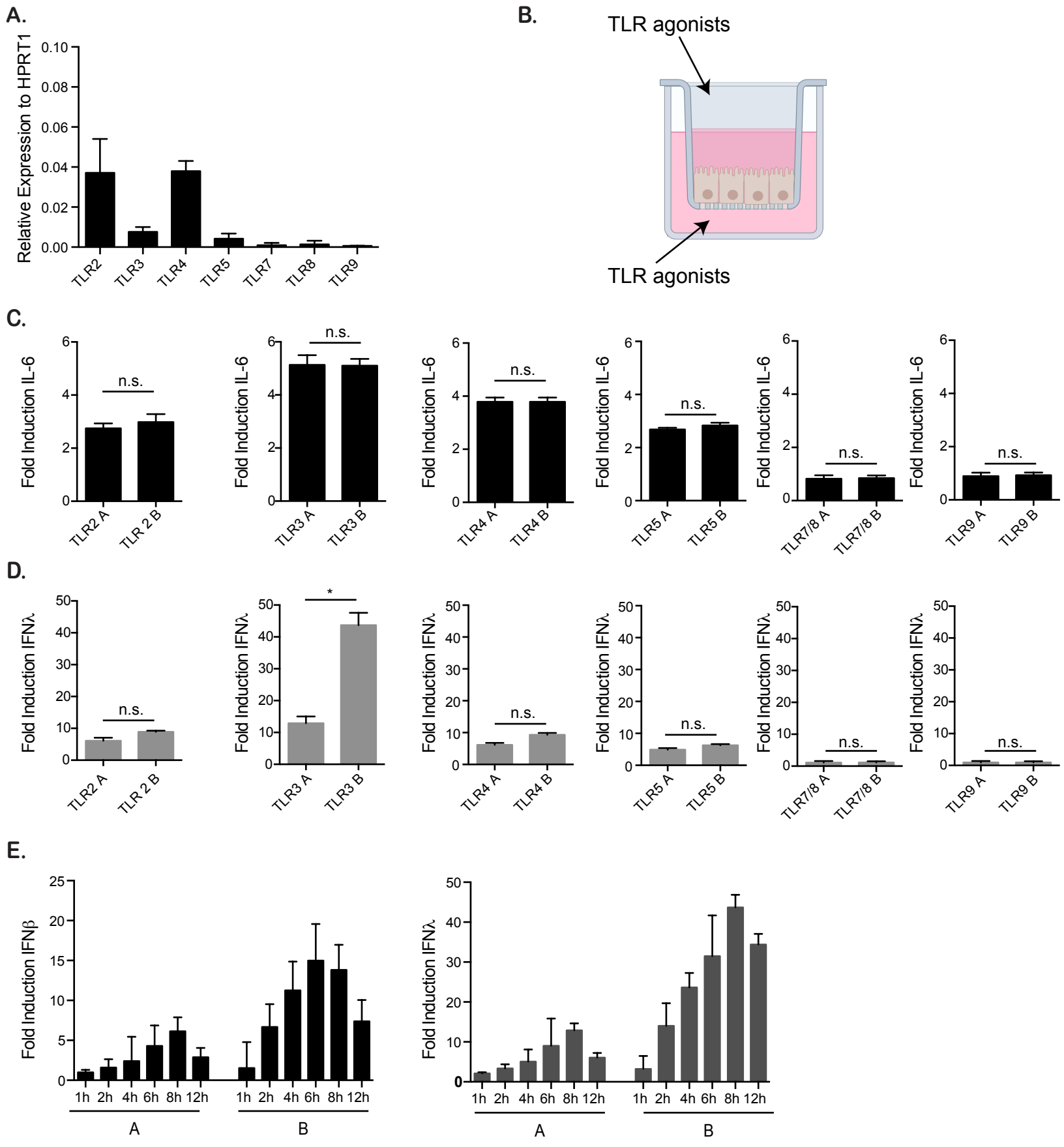
A.
Relative Expression to HPRT1
0.10
0.08
0.06
0.04
0.02
0.00
TLR2
TLR3
TLR4
TLR5
TLR7
TLR8
TLR9
B.
TLR agonists
TLR agonists
C.
Fold Induction IL-6
n.s.
TLR2 A
TLR 2 B
TLR3 A
TLR3 B
TLR4 A
TLR4 B
TLR5 A
TLR5 B
TLR7/8 A
TLR7/8 B
TLR9 A
TLR9 B
D.
Fold Induction IFNλ
*
E.
Fold Induction IFNβ
Fold Induction IFNλ
1h 2h 4h 6h 8h 12h
A
B

Figure 1

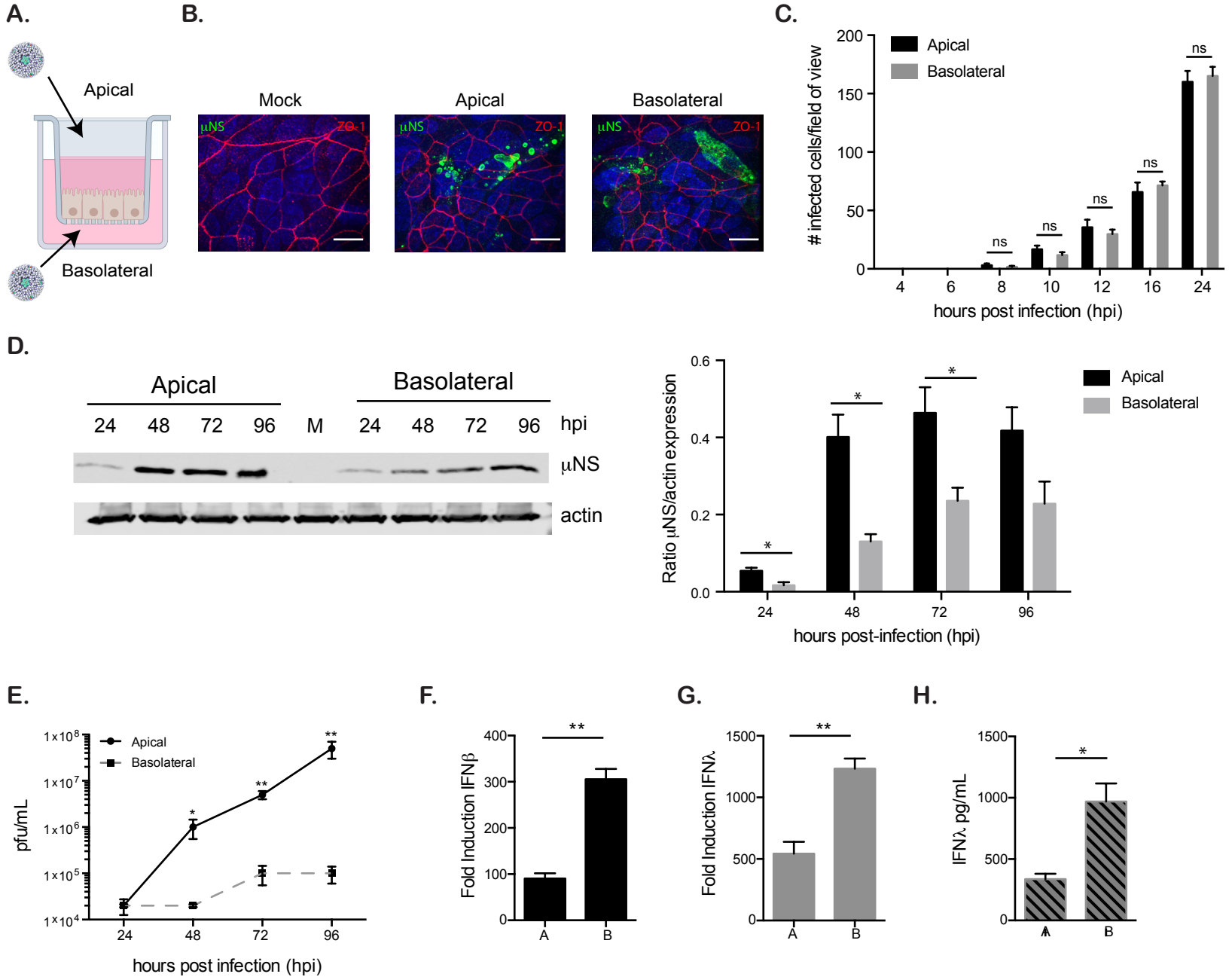
A.
Apical
Basolateral
B.
Mock
Apical
Basolateral
μNS
ZO-1
C.
Apical
Basolateral
infected cells/field of view
hours post infection (hpi)
ns
D.
Apical
Basolateral
24
48
72
96
M
hpi
μNS
actin
Ratio μNS/actin expression
hours post-infection (hpi)
*
E.
Apical
Basolateral
pfu/mL
hours post infection (hpi)
**
F.
Fold Induction IFNβ
A
B
G.
Fold Induction IFNλ
H.
IFNλ pg/mL

Figure 2

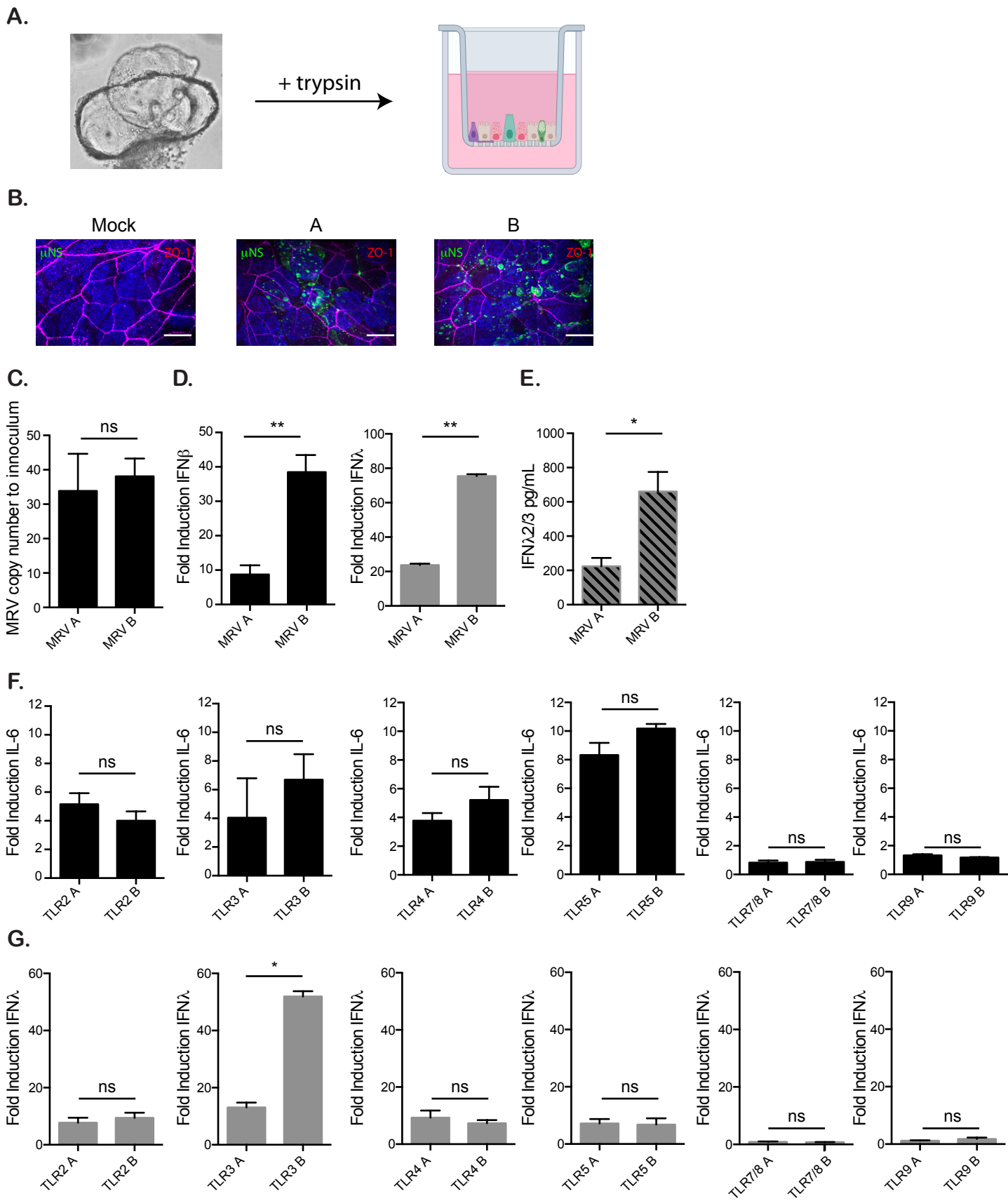
A.
+ trypsin
B.
Mock
A
B
μNS
ZO-1
C.
MRV copy number to innoculum
ns
MRV A
MRV B
D.
Fold Induction IFNβ
**
Fold Induction IFNλ
E.
IFNλ2/3 pg/mL
*
F.
Fold Induction IL-6
TLR2 A
TLR2 B
TLR3 A
TLR3 B
TLR4 A
TLR4 B
TLR5 A
TLR5 B
TLR7/8 A
TLR7/8 B
TLR9 A
TLR9 B
G.

Figure 3

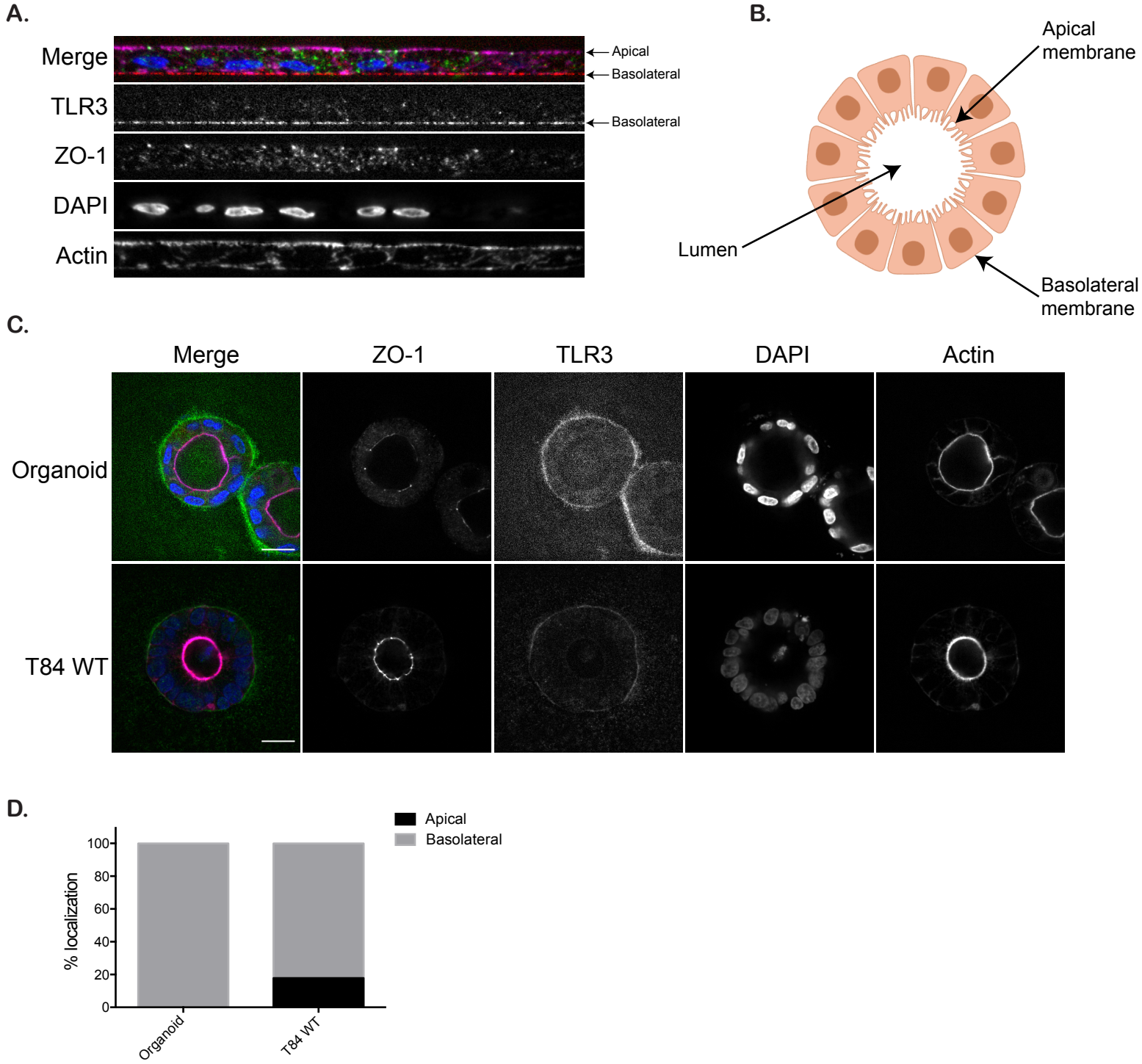
A.
Merge
TLR3
ZO-1
DAPI
Actin
Apical
Basolateral
Basolateral
B.
Apical membrane
Lumen
Basolateral membrane
C.
Merge
ZO-1
TLR3
DAPI
Actin
Organoid
T84 WT
D.
Apical
Basolateral
% localization
100
80
60
40
20
0
Organoid
T84 WT

Figure 4

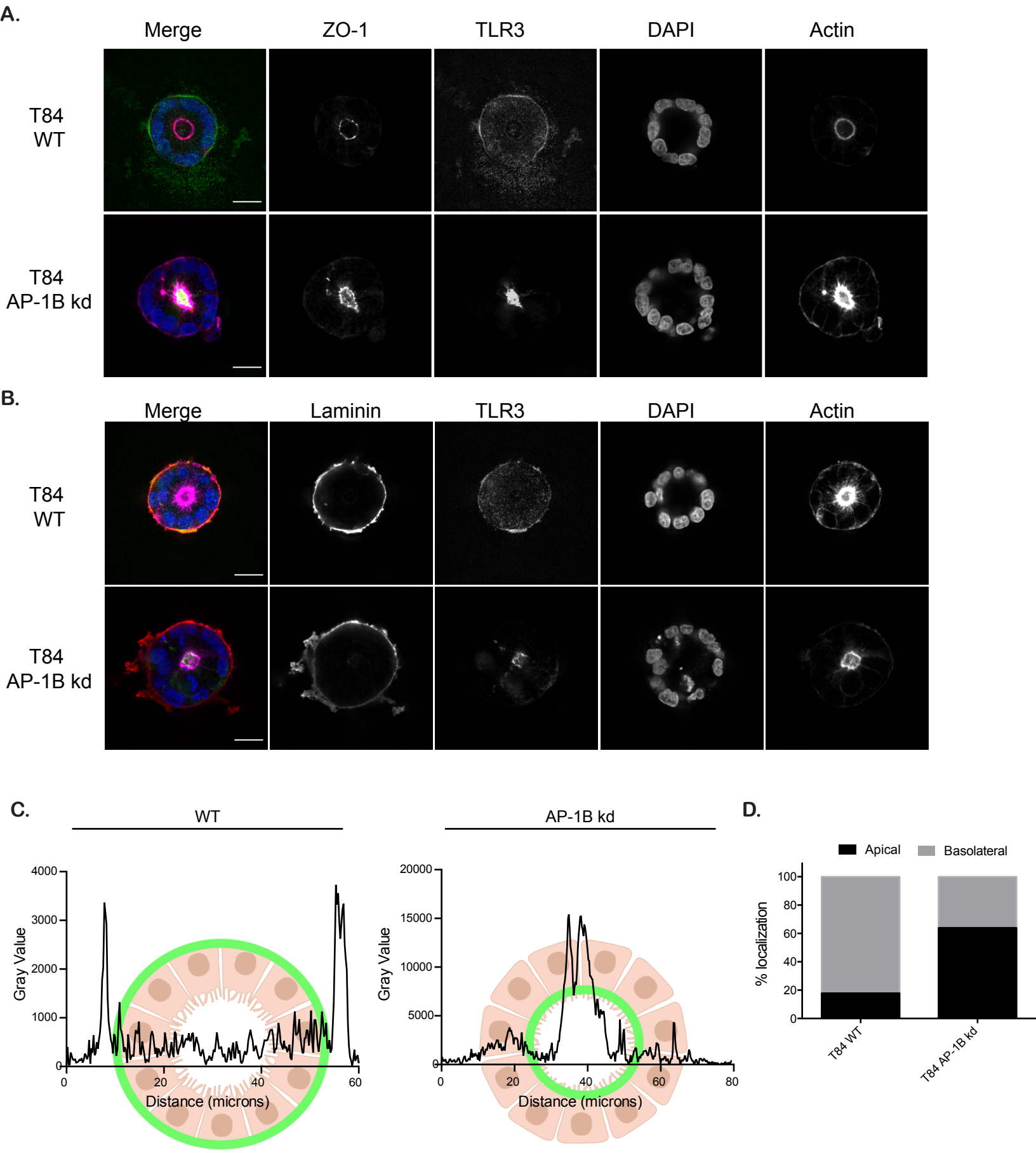
A.
Merge
ZO-1
TLR3
DAPI
Actin
T84 WT
T84 AP-1B kd
B.
Merge
Laminin
TLR3
DAPI
Actin
T84 WT
T84 AP-1B kd
C.
WT
AP-1B kd
Gray Value
Distance (microns)
D.
Apical
Basolateral
% localization
T84 WT
T84 AP-1B kd

Figure 5

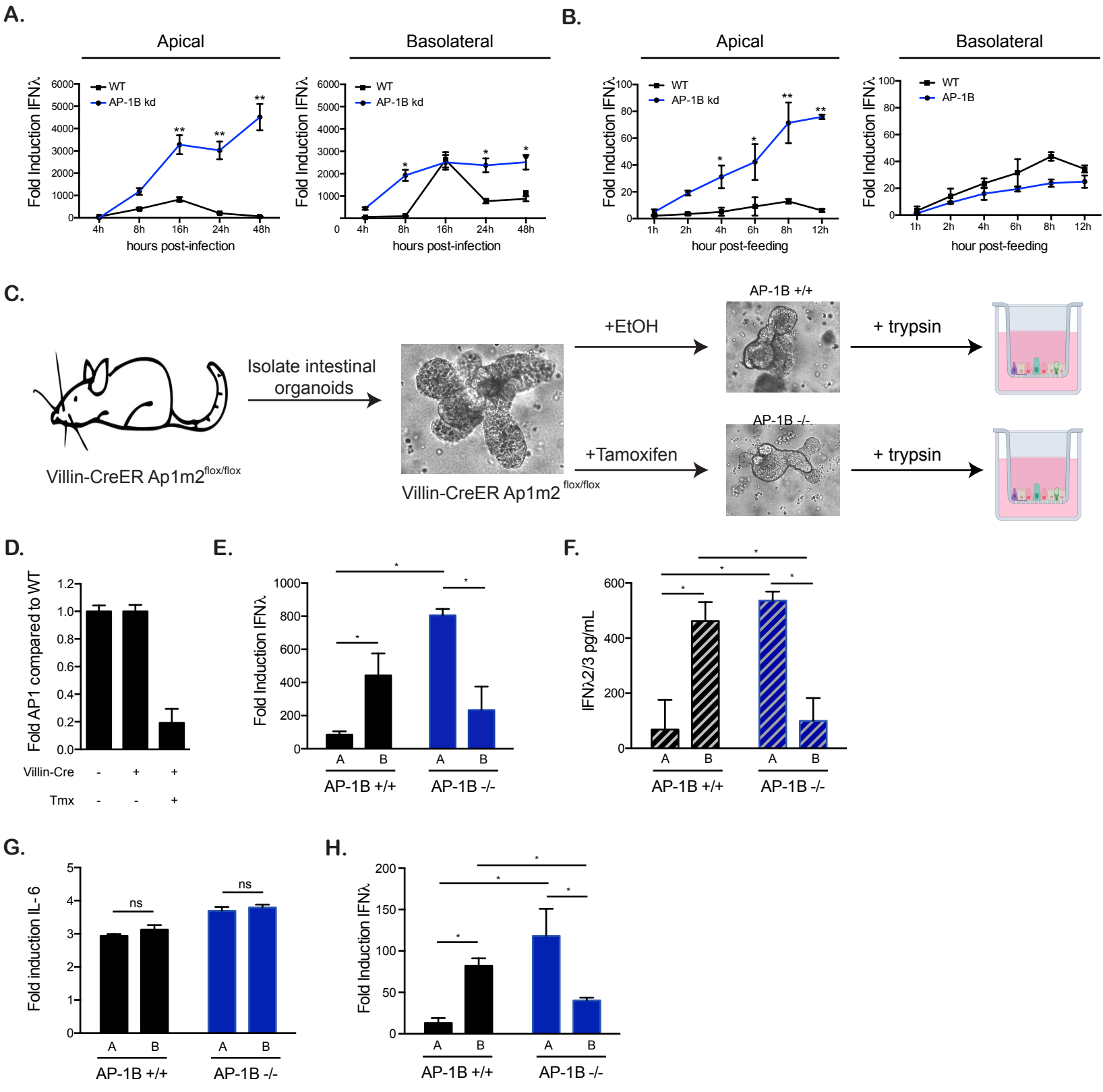
A.
Apical
Basolateral
Fold Induction IFNλ
WT
AP-1B kd
hours post-infection
B.
AP-1B
hour post-feeding
C.
Villin-CreER Ap1m2flox/flox
Isolate intestinal organoids
+EtOH
+Tamoxifen
AP-1B +/+
AP-1B -/-
+ trypsin
D.
Fold AP1 compared to WT
Villin-Cre
Tmx
E.
F.
IFNλ2/3 pg/mL
G.
Fold induction IL-6
ns
H.
A
B

Figure 6